

Consistency of optimizing finite-time Carnot engines with the low-dissipation model in the two-level atomic heat engine

Yu-Han Ma¹, C P Sun^{1,2} and Hui Dong^{1,*}

¹ Graduate School of China Academy of Engineering Physics, Beijing 100193, China

² Beijing Computational Science Research Center, Beijing 100193, China

E-mail: hdong@gscaep.ac.cn

Received 7 September 2021, revised 1 October 2021

Accepted for publication 5 October 2021

Published 12 November 2021



Abstract

The efficiency at the maximum power (EMP) for finite-time Carnot engines established with the low-dissipation model, relies significantly on the assumption of the inverse proportion scaling of the irreversible entropy generation $\Delta S^{(ir)}$ on the operation time τ , i.e. $\Delta S^{(ir)} \propto 1/\tau$. The optimal operation time of the finite-time isothermal process for EMP has to be within the valid regime of the inverse proportion scaling. Yet, such consistency was not tested due to the unknown coefficient of the $1/\tau$ -scaling. In this paper, we reveal that the optimization of the finite-time two-level atomic Carnot engines with the low-dissipation model is consistent only in the regime of $\eta_C \ll 2(1 - \delta)/(1 + \delta)$, where η_C is the Carnot efficiency, and δ is the compression ratio in energy level difference of the heat engine cycle. In the large- η_C regime, the operation time for EMP obtained with the low-dissipation model is not within the valid regime of the $1/\tau$ -scaling, and the exact EMP of the engine is found to surpass the well-known bound $\eta_+ = \eta_C/(2 - \eta_C)$.

Keywords: finite-time thermodynamics, low-dissipation model, quantum heat engine, efficiency at maximum power, irreversible entropy generation

1. Introduction

Converting heat into useful work, a heat engine lies at the core of thermodynamics, both in classical and quantum regimes ([1–4]). Absorbing heat from a hot thermal bath with the temperature T_h , the engine outputs work and release part of the heat to the cold bath with the temperature T_c . The upper limit of the heat engine working between two heat baths is given by the Carnot efficiency $\eta_C = 1 - T_c/T_h$ ([1]). Due to the limitation of the quasi-static cycle with an infinitely-long operation time, the heat engine with Carnot efficiency generally has vanishing output power and in turn is of no practical use. To design the heat engine cycles operating in finite-time, several practical heat engine models have been proposed ([5–7]), such as the endo-reversible model ([8–12]), the linear irreversible model ([13–15]), the stochastic model ([16, 17]), and the low-dissipation model ([18–25]). The efficiency at maximum power

(EMP), is proposed as an important parameter to evaluate the performance of these heat engines in the finite-time cycles.

The utilization of the low-dissipation model ([18–21, 25, 26]) simplifies the optimization of the finite-time Carnot-like heat engines. As the model assumption, the heat transfer between the engine and the bath in the finite-time quasi-isothermal process is divided into two parts as follows

$$Q_{h,c}(\tau_h) = T_{h,c}(\Delta S_{h,c} - S_{h,c}^{(ir)}), \quad (1)$$

where $\Delta S_h = -\Delta S_c = \Delta S$ is the reversible entropy change of the working substance and $S_{h,c}^{(ir)} = \Sigma_{h,c}/\tau_{h,c}$ is the irreversible entropy generation which is inversely proportional to the process time τ_α . Optimizing the output power $P(\tau_h, \tau_c) = [Q_h(\tau_h) + Q_c(\tau_c)]/(\tau_h + \tau_c)$ with respect to the operation time τ_h and τ_c , one gets the optimal operation times ([18]) as

$$\tau_h^* = \frac{2T_h \Sigma_h}{(T_h - T_c)\Delta S} \left(1 + \sqrt{\frac{T_c \Sigma_c}{T_h \Sigma_h}} \right), \quad (2)$$

* Author to whom any correspondence should be addressed.

$$\tau_c^* = \frac{2T_c \Sigma_c}{(T_h - T_c) \Delta S} \left(1 + \sqrt{\frac{T_h \Sigma_h}{T_c \Sigma_c}} \right), \quad (3)$$

and the efficiency at the maximum power η^* bounded by the following inequality as ([7, 18])

$$\eta_- \equiv \frac{\eta_C}{2} \leq \eta^* \leq \frac{\eta_C}{2 - \eta_C} \equiv \eta_+. \quad (4)$$

Due to the simplicity of the model assumption and the universality of the obtained EMP, the low-dissipation model becomes one of the most studied finite-time heat engine models in recent years ([19–25]).

It is currently agreed that ([21, 25–29]) the low-dissipation assumption is valid in the long-time regime of $\tau/t_r \gg 1$, where t_r is the relaxation time characterizing the time scale for the work substance to reach its equilibrium with the heat bath. The quasi-static process is achieved with $\tau/t_r \rightarrow \infty$. The short-time deviation of irreversible entropy generation from the $1/\tau$ -scaling has been clearly demonstrated theoretically ([21]) and experimentally ([29]). And the dissipation coefficient Σ of the $1/\tau$ -scaling is determined by both the coupling strength $\gamma \sim 1/t_r$ to the bath ([21, 29]) and the control scheme ([26, 29]). Such a relation implies that the condition $\tau^*/t_r \gg 1$ is not fulfilled simply and should be justified to reveal the regime of validity. In this paper, we check the consistency of the obtained EMP with a minimal heat engine model consisting of a single two-level system. In section 2, we analytically obtain the regime, where the optimal operation times to achieve EMP are consistent with the low-dissipation assumption. And we further show the possibility of the exact EMP of the engine to surpass the upper bound of EMP, i.e. η_+ , obtained with the low-dissipation model in the large- η_C regime in section 3.

2. Self-consistency of the low-dissipation model in deriving efficiency at maximum power

The two-level atomic heat engine is the simplest quantum engine to demonstrate the relevant physical mechanisms ([21, 26, 30–32]). The energy spacing of the excited state $|e\rangle$ and ground state $|g\rangle$ is tuned by an outside agent to extract work with the Hamiltonian $H = \frac{1}{2} \hbar \omega(t) \sigma_z$, where $\sigma_z = |e\rangle\langle e| - |g\rangle\langle g|$ is the Pauli matrix in the z -direction. The Planck's constant is taken as $\hbar = 1$ in the following discussion for convenience. For the finite-time quasi-isothermal process with the duration τ of the two-level system, the low-dissipation assumption of the $1/\tau$ scaling is valid in the regime $\tilde{\gamma}\tau \gg 1$ ([21]), where $\tilde{\gamma} = t_r^{-1} = 2\gamma T/\omega_0$ in the high temperature regime. Here γ is the coupling strength between the system and the bath with the temperature T and ω_0 is the initial energy spacing of the system during the process.

The finite-time Carnot-like cycle for the two-level atomic heat engine of interest consists of four strokes, two isothermal and two adiabatic processes. The schematic diagram of the cycle is shown in figure 1. In the figure, ω_h^i and ω_h^f (ω_c^i and ω_c^f) are respectively the initial and final energy spacing of the working substance in the high (low) temperature finite-time quasi-isothermal process with duration τ_h (τ_c), which is shown

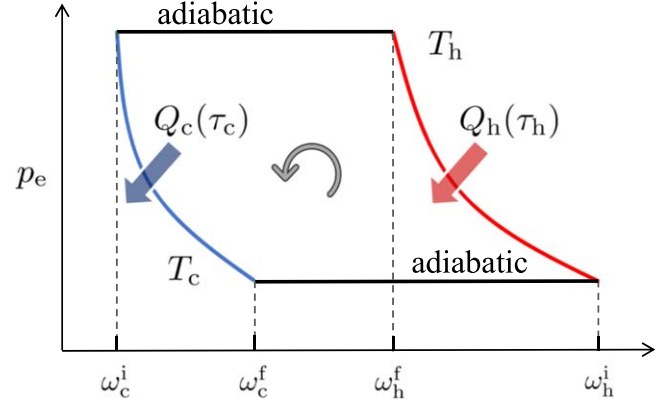


Figure 1. Schematic diagram of the finite-time Carnot-like cycle for a two-level atomic heat engine. The horizontal axis and the vertical axis represent respectively the energy spacing ω and excited state population p_e of the two-level atom. The red (right) and blue (left) solid curves represent the high-temperature and low-temperature finite-time quasi-isothermal processes, respectively. The black (horizontal) solid lines represent the adiabatic processes.

with the red (right) [blue (left)] solid curve. The total operating time per cycle is $t = \tau_h + \tau_c$. Here, we have assumed that the interval of the adiabatic processes, plotted with the black (horizontal) solid lines, are ignored in comparison with τ_h and τ_c ([18, 21]). Such assumption can always be satisfied when the two-level system has no energy level crossing, namely, $\omega(t) = 0$, during the whole cycle. (Since the eigen-states of such systems do not change with time, namely, $|\dot{e}\rangle = 0$ ($|\dot{g}\rangle = 0$), the quantum adiabatic conditions $|\langle e|\dot{g}\rangle/\omega(t)| \ll 1$ and $|\langle g|\dot{e}\rangle/\omega(t)| \ll 1$ are always satisfied with $\omega(t) \neq 0$ ([33, 34]). Therefore, we can tune the energy spacing of the system fast enough to make the corresponding duration of the adiabatic process negligible compared to the time scale $\tilde{\gamma}^{-1}$ of the isothermal process). The quasi-isothermal process retains the normal isothermal process at the quasi-static limit of $T_{h(c)} \rightarrow \infty$.

For simplicity, we focus on the high-temperature regime, where the reversible entropy change ΔS_α and the irreversible entropy generation coefficient Σ_α in equation (1) are analytically written as ([21])

$$\Delta S_\alpha = \frac{[(\omega_\alpha^i)^2 - (\omega_\alpha^f)^2]}{8T_\alpha^2}, \quad \Sigma_\alpha = \frac{(\omega_\alpha^i - \omega_\alpha^f)^2}{4T_\alpha^2 \tilde{\gamma}_\alpha}, \quad (5)$$

where $\alpha = h, c$, $\tilde{\gamma}_\alpha = 1/t_r^{(\alpha)} = 2\gamma_\alpha T_\alpha/\omega_\alpha^i$, and the natural unit $k_B = 1$ and $\hbar = 1$ are used. To obtain the above equations, the relations $\omega_h^i/T_h = \omega_c^f/T_c$, $\omega_h^f/T_h = \omega_c^i/T_c$ have been used in the quantum adiabatic processes ([21, 31]). Substituting equation (5) into equations (2) and (3), we obtain the corresponding optimal operation time τ_α^* for achieving the maximum power with the dimensionless time $\tilde{\tau}_\alpha^* \equiv \tau_\alpha^*/t_r^{(\alpha)} = \tilde{\gamma}_\alpha \tau_\alpha^*$ as

$$\tilde{\tau}_h^* = \frac{2}{\eta_C} \frac{\omega_h^i - \omega_h^f}{\omega_h^i + \omega_h^f} \left[1 + \sqrt{(1 - \eta_C) \frac{\gamma_h}{\gamma_c}} \right], \quad (6)$$

$$\tilde{\tau}_c^* = \frac{2}{\eta_C} \frac{\omega_h^i - \omega_h^f}{\omega_h^i + \omega_h^f} \left[\sqrt{(1 - \eta_C) \frac{\gamma_c}{\gamma_h}} + 1 - \eta_C \right]. \quad (7)$$

The low-dissipation assumption is valid in the regime $\tilde{\tau}_h^* \gg 1$

and $\tilde{\tau}_c^* \gg 1$, namely,

$$1 + \sqrt{(1 - \eta_C) \frac{\gamma_h}{\gamma_c}} \gg \frac{\eta_C \omega_h^i + \omega_h^f}{2 \omega_h^i - \omega_h^f}, \quad (8)$$

$$\sqrt{(1 - \eta_C) \frac{\gamma_c}{\gamma_h}} + 1 - \eta_C \gg \frac{\eta_C \omega_h^i + \omega_h^f}{2 \omega_h^i - \omega_h^f}. \quad (9)$$

The above two inequalities are fulfilled when

$$\eta_C \ll 2 \frac{1 - \delta}{1 + \delta}, \quad (10)$$

where $\delta \equiv \omega_h^f / \omega_h^i$ is the compression ratio of the heat engine cycle in the quasi-isothermal process, and the restriction $\delta > 0$ is required to avoid energy level crossing of the system as we mentioned before. Similar discussion can be applied to the low-temperature regime, where ΔS_α and Σ_α have different expressions ([21]) and equation (10) will change accordingly, please see appendix B for details. The above relation is one of the main results of the current work and reveals the range of η_C in which the low-dissipation model is applicable for finding EMP. The bound for EMP obtained in the low-dissipation regime, as given by equation (4), thus may be not unconditionally applicable to such two-level atomic engine. Indeed, we will show that, out of the low-dissipation regime, the EMP of the two-level atomic heat engine is larger than the upper bound η_+ predicted by the low-dissipation model in the next section.

3. Efficiency at maximum power: beyond the low dissipation model

With the analytical discussion above, we find the EMP obtained with the low-dissipation model is only consistent with the assumption of the low-dissipation model in the low- η_C regime for the two-level system. The question is whether the bound provided by the low-dissipation model, i.e. η_+ , is still the upper bound for the achievable efficiency of the system out of the low- η_C regime. Unfortunately, the answer is no. In this section, we will focus the efficiency at the maximum power in the regime with large η_C .

By numerically simulating the dynamics of the two-level system engine with a different cycle time, we obtain the exact power and efficiency to find the EMP. The results in the large- η_C regime show that: (i) the optimal operation time corresponding to the maximum power of the heat engine does not meet the low-dissipation assumption; (ii) the EMP surpass the upper bound obtained with the low-dissipation model, namely, $\eta_{MP} > \eta_+$.

The dynamics of the two-level atom in the finite-time quasi-isothermal process is given by the master equation as follows ([21])

$$\frac{dp_e(t)}{dt} = -\kappa(t)p_e(t) + C(t), \quad (11)$$

where $p_e(t)$ is the excited state population and $C(t) = \gamma n[\omega(t)]$. $\kappa(t) = \gamma(2n[\omega(t)] + 1)$ is the effective dissipation rate with

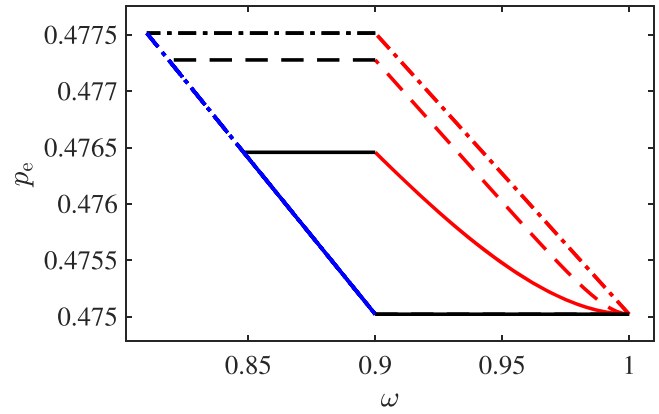


Figure 2. The finite-time Carnot-like cycles for a two-level atomic heat engine with different operation time τ_h . The red (right) curves represent the high-temperature finite-time quasi-isothermal processes with the duration τ_h , while the blue (left) curves represent the low-temperature isothermal processes. The adiabatic processes are plotted with the black (horizontal) lines. The outermost dash-dotted curves relate to the quasi-static cycle with $\tau_h = 200t_r$, while the middle dashed cycle and inner solid cycle are obtained with $\tau_h = 10t_r$ and $\tau_h = 2t_r$, respectively. In this example, we choose $\omega_h^i = 1$, $\omega_h^f = 0.9$, $\gamma_h = 1$, $T_h = 10$, and $T_c = 9$. $t_r = \omega_h^i / (2\gamma_h T_h) = 0.05$ is the relaxation time related to the high-temperature finite-time quasi-isothermal process.

the mean occupation number $n[\omega(t)] = 1/(\exp[\beta\omega(t)] - 1)$ for the bath mode $\omega(t)$. The dissipation rate γ equals to γ_h (γ_c) in the high (low) temperature quasi-isothermal process with the inverse temperature $\beta_h = 1/(k_B T_h)$ ($\beta_c = 1/(k_B T_c)$). The energy spacing of the two-level atom is tuned linearly as $\omega(t) = \omega_h^i + (\omega_h^f - \omega_h^i)t/\tau_h$, $t \in [0, \tau_h]$ in the high-temperature finite-time quasi-isothermal process and as $\omega(t) = \omega_c^i + (\omega_c^f - \omega_c^i)t/\tau_c$, $t \in [\tau_c, \tau_c + \tau_h]$ in the low-temperature finite-time quasi-isothermal process. The population of the two-level system keeps unchanged during the adiabatic processes whose operation time is ignored in comparison with τ_h and τ_c .

In the following simulation, we set $\gamma_h = 1$ and focus on the regime of $\gamma_c/\gamma_h \rightarrow \infty$, i.e. $\Sigma_c/\Sigma_h \rightarrow 0$, where the upper bound $\eta_+ = \eta_C/(2 - \eta_C)$ of EMP of the engine is achieved according to the prediction with the low-dissipation model ([18]). In this regime, the low-temperature quasi-isothermal process approaches the isothermal process quickly enough that the operation time τ_c is further ignored for the optimization of the cycle's output power, and the relaxation time corresponding to the high-temperature quasi-isothermal process is $t_r^{(h)} = \tilde{\gamma}_h^{-1} = \omega_h^i / (2\gamma_h T_h)$. In this case, there is only one relaxation time in the cycle. For brevity, in the following discussion, the superscript of $t_r^{(h)}$ is removed, namely, $t_r^{(h)}$ is denoted as t_r . The optimization of the heat engine cycle is thus simplified as a single parameter optimization problem: find the maximum value P_{\max} of the cycle's output power with respect to τ_h , and obtain the EMP of the engine, $\eta_{MP} \equiv \eta(P = P_{\max})$.

The cycles with different τ_h are illustrated in figure 2, where $\omega_h^i = 1$ and $\omega_h^f = 0.9$ are fixed. The temperatures for the hot and cold bath are chosen as $T_h = 10$ and $T_c = 9$ as an example. The relaxation time is $t_r = \omega_h^i / (2\gamma_h T_h) = 0.05$. The quasi-static cycles with $\tau_h = 200t_r$, $10t_r$ and $2t_r$ are represented by the dash-dotted line, dashed line, and solid line,

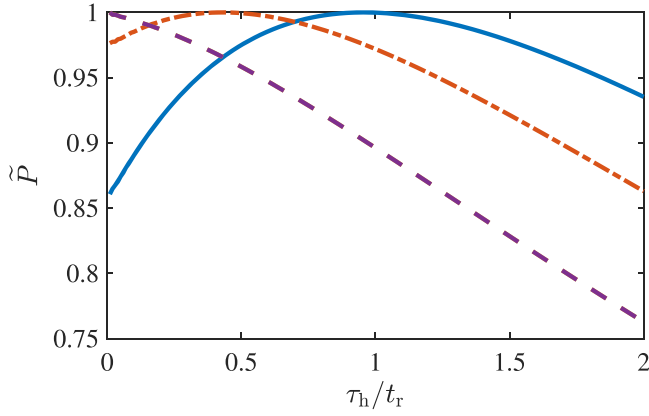


Figure 3. The normalized power of the engine $\tilde{P} = P/P_{\max}$ as a function of τ_h/t_r . The blue solid line, the orange dash-dotted line, and the purple dashed line are respectively obtained with $\eta_C = 0.1$, $\eta_C = 0.12$, and $\eta_C = 0.15$. In this example, we choose $\omega_h^i = 1$, $\omega_h^f = 0.9$, $\gamma_h = 1$, and $T_h = 10$ with changing $T_c = 9, 8.8$ and 8.5 . The relaxation time is $t_r = \omega_h^i/(2\gamma_h T_h) = 0.05$.

respectively. The figure shows that the output work represented by the cycle area decreases with τ_h . Here, we emphasize that t_r is not an independent parameter, and determined by ω_h^i , γ_h , and T_h as $t_r = \omega_h^i/(2\gamma_h T_h)$. The dynamic behavior of the system in finite-time isothermal process is typically characterized by the dimensionless time τ/t_r ([21, 29]). In order to unify the discussion in this section, we did not choose different values of t_r when plotting the figures below, but fix the value of $t_r = 0.05$. (fix the value of ω_h^i , γ_h , and T_h).

In figure 3, we show the normalized power of the engine $\tilde{P} \equiv P/P_{\max}$ as the function of τ_h/t_r with $\eta_C = 0.1$ (blue solid line), $\eta_C = 0.12$ (orange dash-dotted line), and $\eta_C = 0.15$ (purple dashed line). In the simulation, the parameters are set as $\omega_h^i = 1$, $\omega_h^f = 0.9$, and $T_h = 10$ with changing $T_c = 9, 8.8$ and 8.5 . The relaxation time is $t_r = 0.05$. The maximum output power P_{\max} is obtained numerically for different η_C . It is observed from the figure that the dependence of \tilde{P} on operation time τ_h changes with η_C . In the figure, the optimal τ_h^* decreases with η_C and is away from the low-dissipation regime of $\tau_h/t_r \gg 1$, illustrated with the orange dash-dotted line ($\eta_C = 0.12$, $\tau_h^*/t_r \approx 0.5$) and the blue solid line ($\eta_C = 0.1$, $\tau_h^*/t_r \approx 1$). As shown clearly by the purple dashed line with $\eta_C = 0.15$, the maximum power $\tilde{P} = 1$ is achieved in the short-time regime of $\tau_h/t_r \ll 1$, where the $1/\tau$ -scaling of irreversible entropy generation is invalid ([21, 29]).

We show the obtained efficiency η_{MP} at the maximum power of the engine as a function of η_C in figures 4(a) and (b), and plot the corresponding optimal operation time τ_h^* in figure 4(c). We choose the final energy spacing of the two level system as $\omega_h^f = 0.6$ and $\omega_h^f = 0.9$ respectively for (a) and (b), and other parameters are set as $\omega_h^i = 1$, $\gamma_h = 1$, $T_h = 10$. The parameters used in this figure are in the high temperature regime, and the results in the low-temperature regime are illustrated in appendix B. As shown in figures 4(a) and (b), the EMP of the engine η_{MP} (orange solid line) in the large- η_C regime surpasses the upper bound of EMP, $\eta_+ = \eta_C/(2 - \eta_C)$ (black

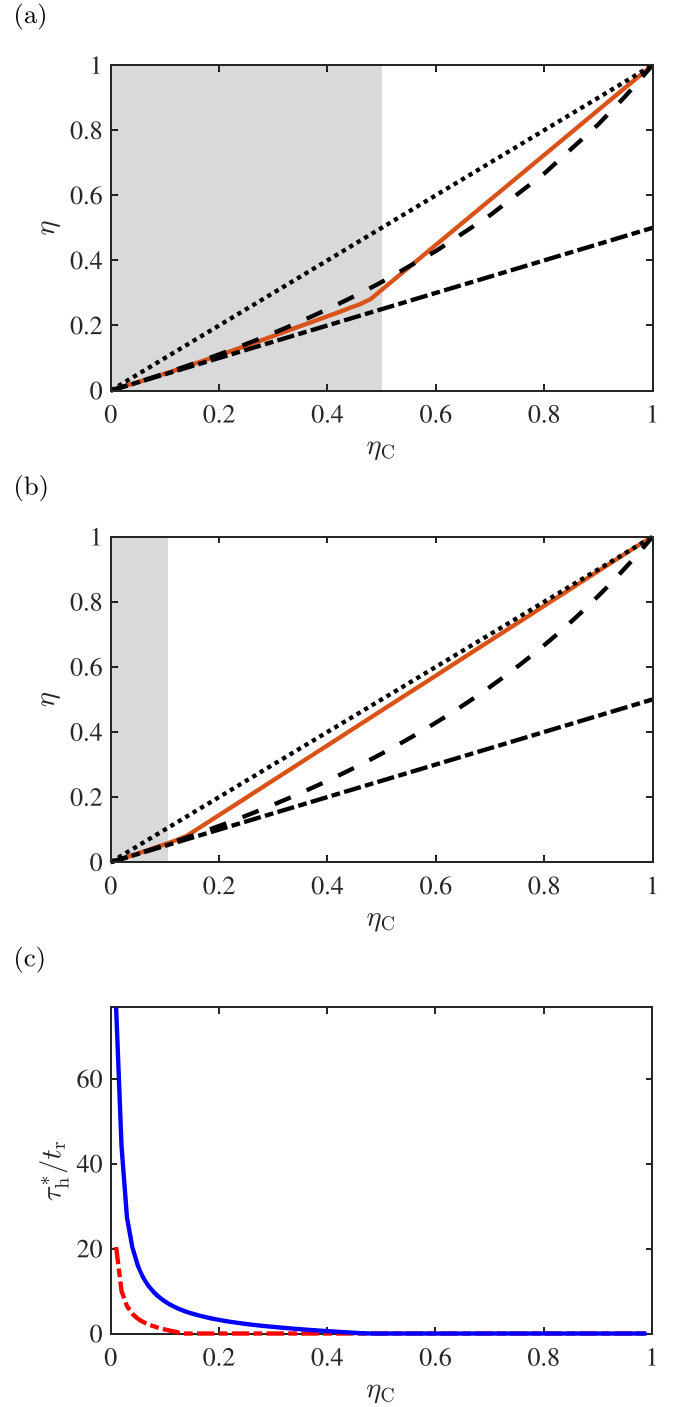


Figure 4. Efficiency at the maximum power η_{MP} (orange solid line) of the heat engine as the function of the Carnot efficiency η_C for different final energy spacing of the two level system (a) $\omega_h^f = 0.6$ and (b) $\omega_h^f = 0.9$. The black dashed line (black dash-dotted line) represents the upper bound η_+ (lower bound η_-) of EMP obtained with the low-dissipation model [equation (4)], and the Carnot efficiency η_C is plotted with the black dotted line. The gray area represents the low-dissipation regime predicted by equation (10). (c) Optimal operation time τ_h^* at the maximum power as the function of η_C . The blue solid curve is obtained with $\omega_h^f = 0.6$ ($\delta = 0.6$) while the red dash-dotted curve is obtained with $\omega_h^f = 0.9$ ($\delta = 0.9$). The other parameters in this figure are chosen as $\omega_h^i = 1$, $\gamma_h = 1$, and $T_h = 10$. The relaxation time is $t_r = \omega_h^i/(2\gamma_h T_h) = 0.05$.

dashed line) obtained with the low-dissipation model. The lower bound of EMP, $\eta_- = \eta_C/2$, obtained with the low-dissipation model is plotted with the black dash-dotted line. The gray area represents the consistent regime as demonstrated by equation (10). The figure shows that η_{MP} is bounded by η_+ and η_- of equation (4) in the gray area with relatively small η_C . Additionally, by comparing (b) and (a) of figure 4, with the larger the compression rate $\delta = \omega_h^f/\omega_h^i$ ($\delta = 0.9$ for (a) and $\delta = 0.6$ for (b)), we illustrate the narrower the range of η_C in which η_{MP} is bounded by η_+ . With the increase of the compression ratio δ , the valid regime of optimization of the engine with the low-dissipation model becomes smaller. And it is consistent with the theoretical analysis of equation (10). Here we emphasize that the gray area only represents the approximate regime where the low-dissipation model is self-consistent, not the exact criterion for η_{MP} to exceed η_+ . Moreover, in the large- η_C regime, the EMP of the heat engine η_{MP} can be analytically obtained as

$$\eta_{MP} = \frac{2\eta_C - 1 + \delta}{1 + \delta}, \quad (12)$$

which increase linearly with η_C as shown by the orange solid lines in figures 4(a) and (b). The detailed derivation and discussion of the above result are presented in appendix A. We note that the achievable regime of the EMP, i.e. $\eta_{MP} \in (\eta_C/2, \eta_C)$, obtained in the current work is consistent with that of the sub-dissipative engines introduced in ([35]).

In figure 4(c), the optimal operation time τ_h^* at the maximum power (blue solid curve for $\omega_h^f = 0.6$ and red dash-dotted curve for $\omega_h^f = 0.9$) decreases monotonically with increasing η_C . For the relatively large η_C , the operation time at maximum power τ_h^* of the engine is not satisfy the low-dissipation assumption holds in the long-time regime of $\tau_h/t_r \gg 1$. Beyond such regime, the irreversible entropy generation will deviate from the $1/\tau$ -scaling ([21, 29]). This explains why η_{MP} is no longer satisfies the bound provided by the low-dissipation model in large- η_C regime, and verifies our analytical analysis in section 2. In addition, one can find in figure 4(c) that the red dash-dotted curve is lower than the blue solid curve. This leads to a narrower parameter range of η_C , in which the optimal operation time τ_h^* satisfies the low-dissipation assumption, for the heat engine with $\omega_h^f = 0.9$ than that with $\omega_h^f = 0.6$. Therefore, the phenomenon that the gray area in figure 4(a) is wider than that in figure 4(b) is explained from the perspective of the operation time.

Here we stress the connection of the current result on η_{MP} in the large- η_C regime with the linear irreversible thermodynamics (LIT) theory: Since the bounds obtained with the low-dissipation model have been tested in the framework of LIT ([36]), it seems that our results contradict linear thermodynamics. However, it should be noted that the equivalence of the low-dissipation model and linear irreversible heat engine model is not unconditional, but depends on specific conditions such as long-time approximation([14]), tight-coupling condition ([36]), and it only holds in the low Carnot efficiency regime with a small temperature difference ([14, 36]). Therefore, our discussion in the large- η_C regime goes beyond the applicable regime of LIT, and it is not

surprising that the obtained results are inconsistent with the predictions of LIT works.

4. Conclusions and discussions

In summary, we checked whether the optimal operation time for achieving the maximum power is consistent with the requirement of the low-dissipation model for the finite-time two-level atomic Carnot-like heat engines in this paper. The low-dissipation model, widely used in the finite-time thermodynamics to study EMP, relies on the assumption that the irreversible entropy generation in the finite-time quasi-isothermal process of duration τ follows the $1/\tau$ scaling in the long-time regime. The operation time for the maximum power obtained from the model should fulfill the requirement of the low-dissipation model assumption. Due to the unknown coefficient of the $1/\tau$ scaling, the consistency of the model in optimizing finite-time Carnot engines had not been tested before.

In this paper, we proved that, in the high-temperature regime, the optimal operation times for a finite-time two-level atomic Carnot engine achieving EMP satisfy the low-dissipation assumption only in the low Carnot efficiency regime of $\eta_C \ll 2(1 - \delta)/(1 + \delta)$, such bound is determined by compression ratio in energy level difference δ of the heat engine cycle. This observation motivated us to check the EMP in the regime with large η_C . We calculated the EMP of the two-level atomic heat engine in the full parameter space of η_C . It is found that, in the large- η_C regime, the true EMP of the heat engine can surpass the upper bound for EMP, i.e. $\eta_+ = \eta_C/(2 - \eta_C)$ obtained with the low-dissipation model. Moreover, in this regime, we found that the true EMP, which is achieved in the short-time limit of $\tau_h/t_r \ll 1$, depends linearly on η_C .

Our study on EMP in the large- η_C regime shall provide a new insight for designing heat engines with better performance working between two heat baths with a large temperature difference. Similar investigation to this work on the two-level atomic heat engine can be extended to some relevant scenarios, such as the optimal cycle of the refrigerator mode beyond the low-dissipation regime. Besides, in addition to affecting the EMP of the heat engine, the short-time effects caused by fast driving may also influence the trade-off between power and efficiency ([20, 21, 27, 28]), which needs further exploration. The predictions of this paper can be tested on some experimental platforms ([29, 37–41]) in the short-time regime.

Acknowledgments

We gratefully acknowledge discussions with D. Xu at Beijing Institute of Technology. We would like to thank the anonymous referees for helpful comments and suggestions. This work is supported by the National Natural Science Foundation of China (NSFC) (Grants No. 11 534 002, No. 11 875 049, No. U1730449, No. U1530401, and No. U1930403), the National Basic Research

Program of China (Grant No. 2016YFA0301201), and the China Postdoctoral Science Foundation (Grant No. BX2021030).

Appendix A. Efficiency at maximum power in the large- η_C regime

The heat absorbed from the high temperature reservoir reads ([21])

$$Q_h = \int \omega_h(t) dp_e = \int_0^{\tau_h} \omega_h(t) \frac{dp_e}{dt} dt. \quad (A1)$$

As shown in figure 3, the maximum power $\tilde{P} = 1$ is achieved in the short-time regime of $\tau_h/t_r \ll 1$ for large η_C . In this case, the excited state population can be approximated as

$$p_e(t/t_r \ll 1) \approx p_e(0) + t \left(\frac{dp_e}{dt} \right)_{t=0}, \quad (A2)$$

where

$$\left(\frac{dp_e}{dt} \right)_{t=0} = -\kappa(0)p_e(0) + C(0) \equiv \zeta. \quad (A3)$$

With this approximation, the heat absorbed is written as

$$\begin{aligned} Q_h &= \int_0^{\tau_h} \omega_h(t) \frac{dp_e}{dt} dt = \int_0^{\tau_h} \omega_h(t) \zeta dt \\ &= \zeta \left[\int_0^{\tau_h} \omega_h^i + (\omega_h^f - \omega_h^i) \frac{t}{\tau_h} dt \right] \\ &= \zeta \tau_h \left(\omega_h^i + \frac{\omega_h^f - \omega_h^i}{2} \right) = \frac{\zeta \tau_h (\omega_h^i + \omega_h^f)}{2}. \end{aligned} \quad (A4)$$

On the other hand, the heat released to the low temperature reservoir is

$$Q_c = \int_{p_e(\tau_h)}^{p_e(0)} \omega_c dp_e. \quad (A5)$$

Since we focus on the regime of $\gamma_c/\gamma_h \rightarrow \infty$, the low-temperature quasi-isothermal process can be considered as the isothermal process with

$$p_e(\omega_c) = \frac{\exp(-\beta_c \omega_c)}{1 + \exp(-\beta_c \omega_c)}, \quad (A6)$$

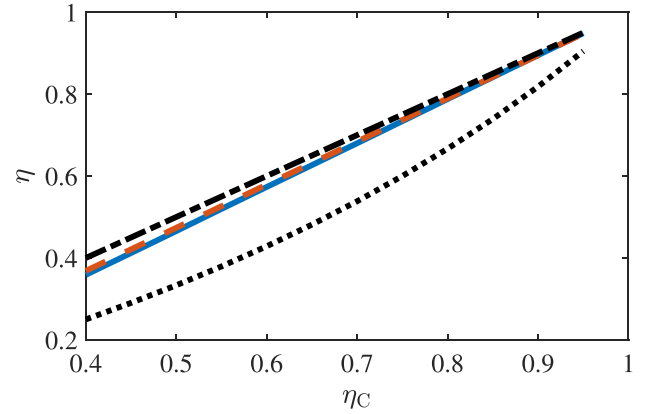
which gives

$$\omega_c = \omega_c(p_e) = -\frac{1}{\beta_c} \ln \left(\frac{p_e}{1 - p_e} \right). \quad (A7)$$

In the two adiabatic processes, we have the following relations

$$p_e(\omega_c^f) = p_e(0), p_e(\omega_c^i) = p_e(\tau_h). \quad (A8)$$

(a)



(b)

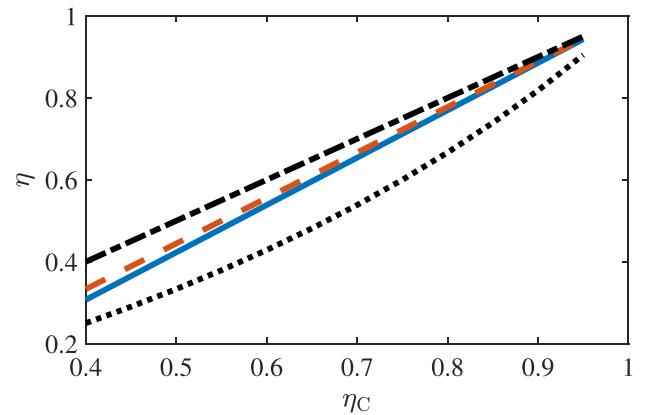


Figure 5. Efficiency at the maximum power η_{MP} (blue solid line) of the heat engine as the function of the Carnot efficiency η_C for different final energy spacing of the two level system (a) $\omega_h^f = 0.9$ and (b) $\omega_h^f = 0.8$. The black dotted line represents the upper bound η_+ and the Carnot efficiency η_C is plotted with the black dash-dotted line. The numerically obtained η_{MP} is plotted with the blue solid line, while the orange dashed line represents the approximated analytical result of equation (A10).

Substituting equation (A7) into equation (A5), we have

$$\begin{aligned} Q_c &= -\frac{1}{\beta_c} \int_{p_e(\tau_h)}^{p_e(0)} \ln \left(\frac{p_e}{1 - p_e} \right) dp_e \\ &= -\frac{1}{\beta_c} \left[\ln(1 - p_e) + p_e \ln \left(\frac{p_e}{1 - p_e} \right) \right]_{p_e(\tau_h)}^{p_e(0)} \\ &= \frac{1}{\beta_c} \frac{d}{dp_e} \left[\ln(1 - p_e) + p_e \ln \left(\frac{p_e}{1 - p_e} \right) \right]_{p_e(0)} \Delta p_e \\ &\quad + O(\Delta p_e^2) \\ &\approx \frac{1}{\beta_c} \ln \left[\frac{p_e(0)}{1 - p_e(0)} \right] \Delta p_e \\ &= -\omega_c[p_e(0)][p_e(\tau_h) - p_e(0)] = -\zeta \tau_h \omega_c^f. \end{aligned} \quad (A9)$$

Here, only the first order of $\Delta p_e = p_e(\tau_h) - p_e(0)$ is kept and

$\omega_c[p_c(0)] = \omega_c^f$ is used by noticing equation (A8). Combining equation (A4) and equation (A9), the EMP of the heat engine in the large- η_C regime ($\tau_h/t_r \ll 1$ regime) is obtained as

$$\begin{aligned}\eta_{MP}(\tau_h/t_r \ll 1) &= \frac{Q_h + Q_c}{Q_h} = \frac{\zeta_{th} \left(\frac{\omega_h^f + \omega_h^i}{2} - \omega_c^f \right)}{\frac{\zeta_{th}(\omega_h^i + \omega_h^f)}{2}} \\ &= \frac{\omega_h^f + \omega_h^i - 2\omega_c^f}{\omega_h^i + \omega_h^f} \\ &= \frac{2\eta_C - 1 + \delta}{1 + \delta},\end{aligned}\quad (A10)$$

where $\delta = \omega_h^f/\omega_h^i$ is the compression ratio, and the relation $\omega_h^i/T_h = \omega_c^f/T_c$ has been used ([21, 31]). As shown in figure 5, in the large- η_C regime, equation (A10) (orange dashed line) matches the numerically obtained EMP (blue solid line) well.

Appendix B. Low-temperature regime

In the low-temperature regime with $\omega/T \gg 1$ (the natural unit $k_B = 1$ and $\hbar = 1$ are used here), the reversible entropy change ΔS_α and the irreversible entropy generation coefficient Σ_α in the long-time limit are analytically written as ([21])

$$\Delta S_\alpha = \beta_\alpha \omega_\alpha^f e^{-\beta_\alpha \omega_\alpha^f} - \beta_\alpha \omega_\alpha^i e^{-\beta_\alpha \omega_\alpha^i}, \quad (B1)$$

and

$$\Sigma_\alpha = \frac{e^{-\beta_\alpha \omega_\alpha^f} - e^{-\beta_\alpha \omega_\alpha^i}}{\tilde{\gamma}_\alpha}, \quad (B2)$$

respectively, with $\alpha = h, c$, $\beta_\alpha = 1/(k_B T_\alpha)$, and $\tilde{\gamma}_\alpha = 1/t_r^{(\alpha)} = \gamma_\alpha T_\alpha / (\omega_\alpha^i - \omega_\alpha^f)$. Substituting equations (B1) and (B2) into equations (2) and (3), we obtain the corresponding optimal operation time τ_α^* for achieving the maximum power with the dimensionless time $\tilde{\tau}_\alpha^* \equiv \tau_\alpha^*/t_r^{(\alpha)} = \tilde{\gamma}_\alpha \tau_\alpha^*$ as

$$\tilde{\tau}_h^* = \frac{2}{\eta_C} \frac{T_h (e^{-\beta_h \omega_h^f} - e^{-\beta_h \omega_h^i})}{\omega_h^f e^{-\beta_h \omega_h^f} - \omega_h^i e^{-\beta_h \omega_h^i}} \left(1 + \sqrt{(1 - \eta_C) \frac{\gamma_h}{\gamma_c}} \right), \quad (B3)$$

$$\tilde{\tau}_c^* = \frac{2}{\eta_C} \frac{T_h (e^{-\beta_h \omega_h^f} - e^{-\beta_h \omega_h^i})}{\omega_h^f e^{-\beta_h \omega_h^f} - \omega_h^i e^{-\beta_h \omega_h^i}} \left(1 - \eta_C + \sqrt{(1 - \eta_C) \frac{\gamma_c}{\gamma_h}} \right). \quad (B4)$$

Here, the relations $\omega_h^i/T_h = \omega_c^f/T_c$, $\omega_h^f/T_h = \omega_c^i/T_c$ have been used in the quantum adiabatic processes. The low-dissipation assumption is valid in the regime $\tilde{\tau}_h^* \gg 1$ and $\tilde{\tau}_c^* \gg 1$, namely,

$$1 + \sqrt{(1 - \eta_C) \frac{\gamma_h}{\gamma_c}} \gg \frac{\eta_C}{2T_h} \frac{[\omega_h^f - \omega_h^i e^{-\beta_h \omega_h^i(1-\delta)}]}{1 - e^{-\beta_h \omega_h^i(1-\delta)}}, \quad (B5)$$

$$\sqrt{(1 - \eta_C) \frac{\gamma_c}{\gamma_h}} + 1 - \eta_C \gg \frac{\eta_C}{2T_h} \frac{[\omega_h^f - \omega_h^i e^{-\beta_h \omega_h^i(1-\delta)}]}{1 - e^{-\beta_h \omega_h^i(1-\delta)}}, \quad (B6)$$

where $\delta = \omega_h^f/\omega_h^i$ is the compression ratio of the heat engine cycle. The above two inequalities are fulfilled when

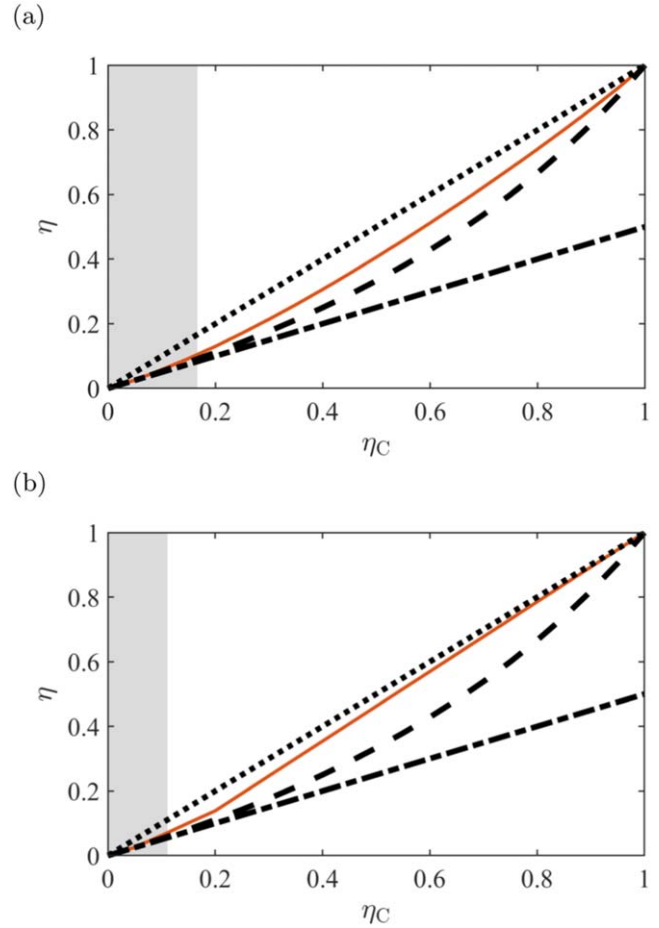


Figure 6. Efficiency at the maximum power η_{MP} (orange solid line) of the heat engine as a function of the Carnot efficiency η_C in the low-temperature regime with $T_h = 0.05$. (a) $\omega_h^f = 0.6$ and (b) $\omega_h^f = 0.9$. The black dashed line (black dash-dotted line) represents the upper bound η_+ (lower bound η_-) of EMP obtained with the low-dissipation model [equation (4)], and the Carnot efficiency η_C is plotted with the black dotted line. The gray area represents the low-dissipation regime predicted by equation (B7). The other parameters in this figure are chosen as $\omega_h^i = 1$ and $\gamma_h = 1$.

$$\eta_C \ll 2 \frac{T_h}{\omega_h^f} \frac{1 - e^{-\beta_h \omega_h^i(1-\delta)}}{1 - \delta^{-1} e^{-\beta_h \omega_h^i(1-\delta)}}. \quad (B7)$$

In this inequality, the right hand term is in the order of T_h/ω_h^f , which is much smaller than 1 in the low-temperature regime. While in equation (10) derived in the high-temperature regime, $2(1 - \delta)/(1 + \delta)$ is in the order of 1. This implies that the range of η_C in which the low-dissipation model is applicable in the low-temperature regime is much narrower than that in the high-temperature regime.

In comparison with the results illustrated in figures 4(a) and (b), we plot η_{MP} (orange solid line) of the heat engine as a function of the Carnot efficiency η_C in the low-temperature regime in figure 6, where we also focus on the regime of $\gamma_c/\gamma_h \rightarrow \infty$ as in the main text. In this figure, except T_h is changed from 10 to 0.05, the values of other parameters are the same as those in figure 4, and the gray area represents the region in equation (B7). As we mentioned in the main text that the gray area only shows the approximate regime where the low-

dissipation model is self-consistent, not the exact criterion for η_{MP} to exceed η_+ . It can be observed in figure 6 that the applicable regime of the low-dissipation model for the two-level atomic heat engine in the low-temperature case is narrower than that in the high-temperature case, as demonstrated in figure 4.

References

- [1] Huang K 2013 *Introduction to Statistical Physics* 2nd edn (Boca Raton, FL: CRC Press)
- [2] Tolman R C and Fine P C 1948 *Rev. Mod. Phys.* **20** 51
- [3] Kosloff R and Levy A 2014 *Ann. Rev. Phys. Chem.* **65** 365
- [4] Binder F, Correa L A, Gogolin C, Anders J and Adesso G (ed) 2018 *Thermodynamics in the Quantum Regime* (Berlin: Springer) (<https://doi.org/10.1007/978-3-319-99046-0>)
- [5] Andresen B, Berry R S, Ondrechen M J and Salamon P 1984 *Acco. Chem. Res.* **17** 266
- [6] Wu C 1999 *Recent Advances in Finite-Time Thermodynamics* (New York: Nova Publishers)
- [7] Tu Z-C 2012 *Chinese Phys. B* **21** 020513
- [8] Reitlinger H B 1929 *Sur l'Utilisation de la chaleur dans les machines a feu* (Paris: Vaillant-Carmanne) Liege: Beranger
- [9] Yvon J 1955 *1st Geneva Conf. Proc. UN*
- [10] Chambadal P 1957 *Recuperation de chaleur a la sortie d' un reacteur, chapter 3* (Paris: Armand Colin)
- [11] Novikov I I 1958 *J. Nucl. Energy II* **7** 125
- [12] Curzon F L and Ahlborn B 1975 *Am. J. Phys.* **43** 22
- [13] den Broeck C V 2005 *Phys. Rev. Lett.* **95** 190602
- [14] Wang Y and Tu Z C 2012 *Phys. Rev. E* **85** 011127
- [15] Izumida Y and Okuda K 2014 *Phys. Rev. Lett.* **112** 180603
- [16] Schmiedl T and Seifert U 2008 *EPL (Europhysics Lett.)* **83** 30005
- [17] Seifert U 2012 *Rep. Prog. Phys.* **75** 126001
- [18] Esposito M, Kawai R, Lindenberg K and den Broeck C V 2010 *Phys. Rev. Lett.* **105** 150603
- [19] Broeck C V D 2013 *EPL* **101** 10006
- [20] Holubec V and Ryabov A 2015 *Phys. Rev. E* **92** 052125
- [21] Ma Y-H, Xu D, Dong H and Sun C-P 2018 *Phys. Rev. E* **98** 042112
- [22] Gonzalez-Ayala J, Guo J, Medina A, Roco J M M and Hernández A C 2020 *Phys. Rev. Lett.* **124** 050603
- [23] Abiuso P and Perarnau-Llobet M 2020 *Phys. Rev. Lett.* **124** 110606
- [24] Ma Y-H 2020 *Entropy* **22** 1002
- [25] Abiuso P, Miller H J D, Perarnau-Llobet M and Scandi M 2020 *Entropy* **22** 1076
- [26] Ma Y-H, Xu D, Dong H and Sun C-P 2018 *Phys. Rev. E* **98** 022133
- [27] Shiraishi N, Saito K and Tasaki H 2016 *Phys. Rev. Lett.* **117** 190601
- [28] Cavina V, Mari A and Giovannetti V 2017 *Phys. Rev. Lett.* **119** 050601
- [29] Ma Y-H, Zhai R-X, Chen J, Dong H and Sun C P 2020 *Phys. Rev. Lett.* **125** 210601
- [30] Geva E and Kosloff R 1992 *J. Chem. Phys.* **96** 3054
- [31] Quan H T, Liu Y-X, Sun C P and Nori F 2007 *Phys. Rev. E* **76** 031105
- [32] Su S, Chen J, Ma Y, Chen J and Sun C 2018 *Chinese Phys. B* **27** 060502
- [33] Albash T, Boixo S, Lidar D A and Zanardi P 2012 *New J. Phys.* **14** 123016
- [34] Dann R, Levy A and Kosloff R 2018 *Phys. Rev. A* **98** 052129
- [35] Yang W and Zhan-Chun T 2013 *Commun. Theor. Phys.* **59** 175
- [36] Izumida Y and Okuda K 2012 *EPL (Europhysics Letters)* **97** 10004
- [37] Martínez I A, Roldán É, Dinis L, Petrov D, Parrondo J M R and Rica R A 2015 *Nat. Physics* **12** 67
- [38] Rosznagel J, Dawkins S T, Tolazzi K N, Abah O, Lutz E, Schmidt-Kaler F and Singer K 2016 *Science* **352** 325
- [39] Deng S, Chenu A, Diao P, Li F, Yu S, Coulamy I, del Campo A and Wu H 2018 *Science Advances* **4** eaar5909
- [40] Albay J A C, Wulaningrum S R, Kwon C, Lai P Y and Jun Y 2019 *Phys. Rev. Res.* **1** 033122
- [41] Bouton Q, Nettersheim J, Burgardt S, Adam D, Lutz E and Widera A 2021 *Nat. Commun.* **12** 2063